Electrochimica Acta 56 (2011) 2990–2998

Contents lists available at ScienceDirect

Electrochimica Acta

journal homepage: www.elsevier.com/locate/electacta

Amphiphilic amido-amine as an effective corrosion inhibitor for mild steel exposed to CO_2 saturated solution: Polarization, EIS and PM-IRRAS studies

M.P. Desimone[a,*], G. Grundmeier[b], G. Gordillo[c], S.N. Simison[a]

[a] División Corrosión, INTEMA, UNMdP-CONICET, Juan B. Justo 4302, B7608FDQ, Mar del Plata, Argentina
[b] Department of Technical and Macromolecular Chemistry, University of Paderborn, Warburger Str. 100, D-33098 Paderborn, Germany
[c] INQUIMAE (CONICET) - DQIAQF – Facultad de Ciencias Exactas y Naturales, Universidad de Buenos Aires, Ciudad Universitaria, Pabellón 2, Buenos Aires, Argentina

ARTICLE INFO

Article history:
Received 18 October 2010
Received in revised form
30 December 2010
Accepted 3 January 2011
Available online 15 January 2011

Keywords:
CO_2 corrosion
Mild steel
Polarization curves
EIS
PM-IRRAS

ABSTRACT

The corrosion behavior of mild steel in CO_2-saturated 5% NaCl solution with N-[2-[(2-aminoethyl) amino] ethyl]-9-octadecenamide corrosion inhibitor at 25 °C has been studied by using potentiodynamic polarization, electrochemical impedance spectroscopy (EIS) and Polarization Modulation Infrared Reflection Absorption Spectroscopy (PM-IRRAS) measurements. Both potentiodynamic polarization and EIS measurements reveal that this amido-amine precursor inhibits the carbon steel corrosion and the inhibition efficiency increases with increasing the inhibitor concentration. The corrosion inhibitor exhibits high corrosion efficiencies as a mixed-type inhibitor, with a predominant influence on the anode process. The organic inhibitor acts blocking surface sites at low concentrations and by modifying the adsorption mechanism forming a protective barrier against corrosive ions at high concentrations. EIS results show that the mechanism of its corrosion inhibition at concentrations higher than 0.82×10^{-5} M is by forming a protective bilayer with small pore sizes that hinders the passage of the reactive species. PM-IRRAS measurements demonstrate that the inhibitor is chemisorbed to surface steel. Therefore, its spectrum reveals that the inhibitor monolayer has an amorphous structure.

1. Introduction

Corrosion has a very important economic impact in the petroleum industry. Carbon dioxide (CO_2) is a naturally occurring constituent in oil and gas production and is found in amounts varying from trace levels to as much as 50%. Besides, CO_2 could be intentionally added as part of secondary enhanced oil recovery processes. Dissolved carbon dioxide in the produced brines is very corrosive to carbon and low alloy steel tubulars employed in the process equipment in this industry. CO_2 corrosion has become of great concern mainly to the increasing production of water due to the ageing of fields as well as the implementation of water-flooding systems for enhanced oil recovery. These problems have caused the consideration of many corrosion control methods and research in various oilfields around the world. The most popular control method is the use of organic inhibitors in combination with low alloy or C–Mn steels. It is generally accepted that organic molecules inhibit corrosion via adsorption at the metal–solution interface. The mode of adsorption is dependent on the following factors: structure of the molecule, solution chemistry, characteristics of the metal surface, and electrochemical potential at the interface. Four primary modes of adsorption are associated with organic compounds at surfaces: electrostatic adsorption, π-back bonding, chemisorption, and organometallic complex formation. In the study and prevention of corrosion, an understanding of the mechanism of both corrosion and corrosion inhibition is essential.

Organic nitrogen-based compounds such as imidazolines, amides, amido-amines and amines, and their salts have been used successfully as corrosion inhibitors in oilfield systems. Nowadays, there is not a conclusive answer about the stability (hydrolysis) of imidazolines and imidazoline formulated products and the activity of the hydrolyzed products. The hydrolysis of imidazoline-based corrosion inhibitors is considered negligible under most conditions, but the presence of significant amounts of water and high temperatures can hydrolyze them to form their amide precursor. There are controversial results in literature about the performance of imidazoline and amide based products. Martin et al. [1] studied several amides and imidazolines compounds, some of them prepared in the laboratory and others obtained from commercial sources. According to these authors, the studied imidazolines, whether alone or formulated into corrosion inhibitors, are spontaneously and fairly rapidly converted into their amide precursor. Therefore, the performance of inhibitors formulated with an imidazoline or its amide precursor would be similar. They suggest that these results can be used to reduce the cost of the imidazoline-based corrosion inhibitor

* Corresponding author. Tel.: +54 223 481 6600x244; fax: +54 223 481 0046.
E-mail addresses: desimone.mariela@gmail.com, mdesimone@fi.mdp.edu.ar (M.P. Desimone).

0013-4686/$ – see front matter © 2011 Elsevier Ltd. All rights reserved.
doi:10.1016/j.electacta.2011.01.009

by replacing the imidazoline with its cheaper amide precursor. Butler et al. [2] reported a high-rate conversion (up to 80%) from imidazoline to amide within a period of 2–9 days under atmospheric conditions because of the low stability of the imidazoline cycle. Jovancicevic et al. [3] studied the effect of hydrolysis of imidazoline on corrosion inhibition by using the Linear Polarization Resistance (LPR) method with the Rotating Cylinder Electrode (RCE) assembly in CO_2 containing brines. They found that the hydrolysis of saturated straight chain imidazolines plays an important role in their inhibition. Thus, under those test conditions, stearic imidazoline hydrolyzes fairly rapidly to a product equivalent in performance to stearic amide.

A detailed understanding of the mechanism of adsorption for corrosion inhibitors requires the characterization of corrosion inhibitor films by using surface analytical techniques. Electrochemical Impedance Spectroscopy (EIS) has proved to be a powerful technique to study corrosion processes and inhibitor performance in different environments [4–6]. For metal substrate supported organic thin films, one of the IR techniques most widely used is the Polarization Modulation Infrared Reflection Absorption Spectroscopy (PM-IRRAS) method [7]. The surface sensitivity of PM-IRRAS is very high, allowing characterizing of adsorbed molecules monolayers.

Taking into account that amido-amine compounds can be effective and economic corrosion inhibitors, a clear understanding of the mechanism of action of the corrosion inhibition process is still needed for reliable field applications [8]. At present, there is no general or specific explanation reported yet for the performance of the amide precursor N-[2-[(2-aminoethyl) amino] ethyl]-9-octadecenamide as corrosion inhibitor in mild steel in CO_2 saturated media at 25 °C. Because of that, it is of interest to carry out a systematic study. In the present work, PM-IRRAS, EIS technique and some electrochemical DC methods were employed in order to go forward to clarify how this inhibitor works.

2. Experimental

2.1. Materials and medium

A mild steel SAE/AISI grade 1018 (Metal Samples) was used as working electrode. It was machined into 7 mm diameter bar, cut and mounted with epoxy resin in a disc electrode holder with an exposed area of 0.38 cm^2. Electrical contact between the sample and holder was obtained with silver loaded epoxy resin.

For the electrochemical tests, surfaces were polished with 600-grit SiC paper, washed with distilled water and rinsed with ethanol. Experiments were conducted at atmospheric pressure, 25 °C and under low speed magnetic stirring. Three-electrode jacketed test cells with a working volume of 0.5 l and a concentric Pt ring as counter electrode were employed. A saturated calomel electrode (SCE) was chosen as reference. Testing solution was deaerated by purging CO_2 (99.95%) for 2 h prior to the experiments. The oxygen concentration of the solution was measured with a Fibox 3-trace v6 (PreSens GmbH) instrument with an accuracy of 0.3 parts per billion (ppb), and it was kept below 40 ppb during the experiments. Test solution was 5 wt% NaCl (analytical-reagent grade) saturated with deoxygenated CO_2. A positive pressure of deoxygenated CO_2 was maintained throughout the experiments to avoid air ingress. All the electrochemical experiments were performed at atmospheric pressure. The pH was adjusted to 6 adding 10–15 ml of deoxygenated 1.0 M $NaHCO_3$.

The inhibitor used in this study was N-[2-[(2-aminoethyl) amino] ethyl]-9-octadecenamide (AAOA) whose molecular formula is shown in Fig. 1. AAOA was synthesized from oleic acid and diethylenetriamine according to Ref. [9]. The target compound

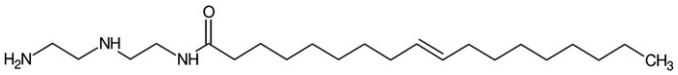

Fig. 1. N-[2-[(2-aminoethyl) amino] ethyl]-9-octadecenamide.

was successfully synthesized as can be seen from the IR spectrum (showed as reference in Fig. 7). A stock solution was prepared by dissolving AAOA in isopropanol to 0.625 M. The inhibitor was used in a concentration range of 6.8×10^{-7} to 5.5×10^{-5} M.

The inhibitor was added at the beginning of the experiments and the formation of the inhibitor film was evaluated after 2 h of immersion period. The samples were kept at open circuit potential (E_{corr}) during their exposure to the corrosive medium.

2.2. Electrochemical measurements

A Voltalab PGZ 402 unit was used for electrochemical measurements. The linear polarization method was used for the determination of the polarization resistance (*Rp*) by polarizing the working electrode ±0.010 V vs. E_{corr} with a sweep rate of 10^{-4} V s^{-1}. The slope of the tangent at the origin provided the value of *Rp*. EIS was measured at the E_{corr} using an applied potential of ±0.01 V rms with a frequency range of 100,000–0.01 Hz. The corrosion potential was also monitored before and after DC and AC analyses.

Potentiodynamic polarization curves were drawn at the end of the experiments, with a sweep rate of 10^{-3} V s^{-1}. The scanning range was from E_{corr} to −0.45 V (SCE) for cathodic curves and from E_{corr} to 0.45 V (SCE) for anodic ones. The electrochemical data were analyzed using the VoltaMaster 4 and Zview 2 software.

At least four replicas were tested for each experimental condition and the surface morphology of the mild steel samples after immersion in CO_2 saturated solution in the absence and presence of AAOA, was examined using an Olympus MG optical microscope.

2.3. Polarization modulation infrared reflection absorption spectroscopy (PM-IRRAS)

Chemical identification of the adsorbed AAOA layer was done *ex situ* employing PM-IRRAS. Measurements were performed using a step scan interferometer (Bruker Vertex 70) with a resolution of 4 cm^{-1} and an angle of incidence of 80° relative to the substrate surface normal. For p-polarization of the IR light, an aluminum wire grid was used and modulated at 50 kHz with a ZnSe photoelastic modulator (PEM, Bruker PMA-50). Light reflected from the sample was focused with a ZnSe lens onto a cryogenic mercury cadmium telluride (MCT) detector. All presented spectra were averaged from 1024 scans. PM-IRRAS spectra were processed using the OPUS 6.5 software.

Before tests, samples were abraded using wet emery papers up to 2500 mesh. Then, they were polished with polycrystalline diamond suspension having a particle size of 1 μm. The surface was rinsed with distilled water and ethanol, and cleaned in ethyl alcohol for 10 min using an ultrasonic bath. After that, samples were immersed in the inhibited solution. Spectrum of each sample was obtained in three different conditions: (i) before immersion into the solution, (ii) dried with a stream of pure nitrogen after 2 h of inhibition, and (iii) washed with a small amount of ethanol and dried with pure nitrogen after recording the previous spectrum.

Surface analyses were undertaken immediately after the test was finished.

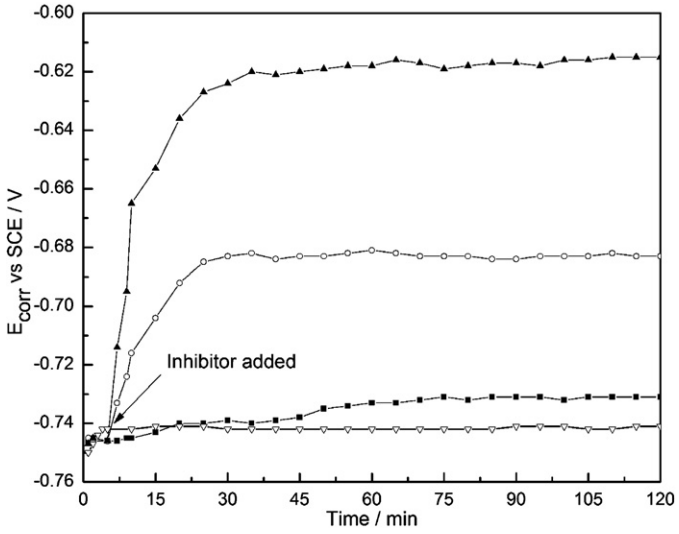

Fig. 2. Variation of E_{corr} with time of steel electrodes in a CO_2 saturated solution in absence and presence of the inhibitor at 25 °C: (▽) 0 M, (■) 0.14×10^{-5} M, (○) 0.82×10^{-5} M, (▲) 2.72×10^{-5} M.

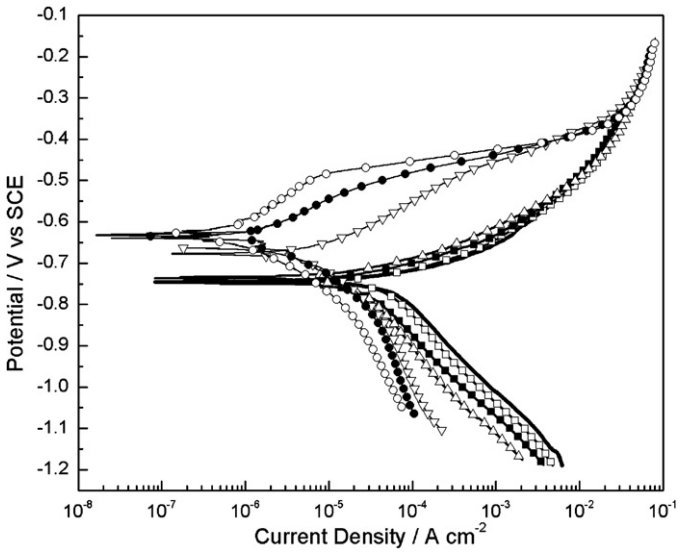

Fig. 3. Polarization curves of mild steel exposed in a CO_2-saturated 5% NaCl solution containing different concentrations of inhibitor at 25 °C: (—) 0 M, (□) 0.07×10^{-5} M, (■) 0.14×10^{-5} M, (△) 0.27×10^{-5} M, (▽) 0.82×10^{-5} M, (●) 1.36×10^{-5} M and (○) 5.44×10^{-5} M.

3. Results and discussion

3.1. DC electrochemical results

Linear polarization resistance and EIS techniques require the corrosion potential to be stable during the measurements. Therefore, special care is taken in attaining the stability of E_{corr} before each polarization or impedance run. Moreover, measurements of E_{corr} variations with time are important to evaluate the partial or complete inhibition and also to determinate the inhibitor-threshold concentrations [10]. The evolution of E_{corr} of carbon steel electrodes with time when different concentrations of the inhibitor are added at 25 °C is shown in Fig. 2.

The steady-state E_{corr} value is achieved after about 30 min of immersion. A positive shift in the corrosion potential is normally observed when applying corrosion inhibitors on mild steel in CO_2 containing brines [11]. For concentrations lower than 0.14×10^{-5} M of AAOA, the shift in the corrosion potential is less than 0.010 V (SCE) within the first 2 h after inhibitor addition. In contrast, for concentrations of the AAOA inhibitor of 0.82×10^{-5} M and higher, E_{corr} significantly increases within a few minutes starting from the electrode immersion. The steady state corrosion potentials are -0.683 ± 0.004 V (SCE) and -0.615 ± 0.001 V (SCE) for 0.82 and 2.72×10^{-5} M, respectively.

For all the experimental conditions, a uniform and regular attack is observed by optical microscopy. Table 1 shows E_{corr}, Rp, corrosion rate (C_R) and the inhibition efficiency results for AISI 1018 steel for different concentrations of inhibitor at 25 °C after 2 h of immersion. The corrosion current density (j_{corr}) is calculated applying the Stearn Geary equation ($B = 0.022$ V) [12]. For each concentration, C_R is calculated using the Faraday law and the iron density. All the recorded j_{corr} values (expressed in $\mu A\,cm^{-2}$) are converted into the C_R in $\mu m\,y^{-1}$ (micrometer per year, the penetration rate of corrosion through a metal) using the expression:

$$C_R = 3.27 j_{corr} \left(\frac{M}{nd}\right) \quad (1)$$

where M is the atomic weight of Fe (55.85 g), n the number of electrons transferred in the corrosion reaction ($n = 2$) and d is the iron density ($7.88\,g\,cm^{-3}$).

The inhibition efficiency (IE) is calculated as follows:

$$IE\,(\%) = \frac{Rp_{inh} - Rp_0}{Rp_{inh}} \quad (2)$$

where Rp_0 and Rp_{inh} are the uninhibited and inhibited polarization resistant, respectively.

As it can be seen, the inhibition efficiency increases strongly up to a concentration of the inhibitor of 0.82×10^{-5} M. With 5.44×10^{-5} M inhibitor addition the corrosion rate decreases by two orders of magnitude relative to the uninhibited corrosion rate. Maximum inhibition efficiency is achieved at 2.72×10^{-5} M and a further increase in concentration does not cause any appreciable change in the performance of the inhibitor.

Typical polarization curves of AISI 1018 with different concentrations of inhibitor are shown in Fig. 3.

It can be observed that the presence of the AAOA amido-amine inhibits the anodic as well as the cathodic reactions. The corrosion inhibition can be attributed to the adsorption of the AAOA at the steel/solution interface.

At low concentrations (lower than 0.27×10^{-5} M) the inhibitor acts over the cathodic and the anodic reactions almost equally, without a significant change neither in the E_{corr} nor in Tafel slopes. The decrease in the corrosion rate associated with a shift of both cathodic and anodic branches of the polarization curves towards lower current densities without a change in the corrosion potential indicates that the amido-amine acts blocking the active sites available for corrosion reaction. According to Cao [13], the invariability of E_{corr} with the inhibitor addition could be associated with a geometric blocking mechanism of both types of sites.

Table 1
Electrochemical measurements for mild steel in a CO_2 media containing different concentrations of the inhibitor for 2 h at 25 °C.

Concentration ($\times 10^{-5}$ mol dm^{-3})	E_{corr} (V vs SCE)	Rp (Ω cm^2)	C_R ($\mu m\,y^{-1}$)	IE (%)
0	−0.741	331	770	–
0.07	−0.742	457	558	28
0.14	−0.731	602	423	45
0.27	−0.727	940	271	65
0.82	−0.683	3291	77	90
1.36	−0.625	16662	15	98
2.72	−0.615	21879	12	99
4.08	−0.614	26378	10	99
5.44	−0.606	33167	8	99

Table 2
Electrochemical parameters calculated from polarization measurements on the steel electrode in CO_2 saturated solution with different inhibitor concentrations at 25 °C.

Concentration ($\times 10^{-5}$ mol dm^{-3})	j_{corr} (μA cm^{-2})	C_R (μm y^{-1})	EI (%)
0	65	748	–
0.07	50	581	22
0.14	38	441	41
0.27	25	291	61
0.82	6.3	73	90
1.36	1.3	16	98
2.72	0.79	9	99
4.08	0.51	6	99
5.44	0.45	5	99

Table 3
Frequency values corresponding to the maximum of the imaginary component of the impedance in a CO_2-saturated 5% NaCl solution with different inhibitor concentrations at 25 °C.

Concentration ($\times 10^{-5}$ mol dm^{-3})	f′ (Hz)
0	1.58
0.07	1
0.14	1
0.27	0.8
0.82	0.39
1.36	0.0633
2.72	0.04
5.44	0.0316

At concentrations of inhibitor higher than 0.27×10^{-5} M, a great change in Tafel slopes is observed jointly with a more significant decrease of anodic currents in comparison with cathodic ones. The anodic shift in E_{corr} is in agreement with the preferential inhibition of the anodic reaction which could be related to the formation of a protective film [3]. Polarization curves shows that the studied compound is an inhibitor of the mixed type with the predominant influence on the anode process.

The above results hint at a change of the adsorption behavior with the concentration of the studied inhibitor. The most probable rationale for the above observation could be attributed to the blocking of reaction sites primarily by physisorption in the lower concentration range. At higher concentrations, the anodic sites could be also blocked by chemisorption of the electron rich amine or carbonilic moieties to the positive centers of the metal including Fe(II) [14].

For 0.82×10^{-5} M and higher concentrations of the inhibitor and potentials higher than −0.490 V (SCE), there is a change in the slope of the anodic curve and the currents abruptly increase. The potential at which an abrupt increase of current density occurs when polarization potential reaches a relatively positive value is usually defined as the desorption potential, E_{des}. This behavior has been reported for iron in halide containing inhibitor solutions and is ascribed to desorption of adsorbed inhibitor with potential [15–17]. This process will result in the surface coverage decrease to zero ultimately and metal becomes "naked" to solution as is the case without inhibitor. Therefore, it is observed that at potentials higher than −0.350 V (SCE) the polarization curves in absence and presence of inhibitor almost coincide. E_{des} and the desorption rate increase with the inhibitor concentration, which is associated with a more adherent inhibitor film [18].

Potentiodynamic curves obtained for mild steel electrode in the brine show no Tafel dependence in anode region so corrosion current is determined graphically from the cathodic polarization curve. The polarization parameters are shown in Table 2.

The inhibition efficiency, *IE*, can also be calculated from the electrochemical relation:

$$IE\,(\%) = \frac{jcorr_0 - jcorr_{inh}}{jcorr_0} \quad (3)$$

where $jcorr_0$ and $jcorr_{inh}$ are the corrosion current density values without and with inhibitor, respectively.

These results are in good agreement with those calculated from linear polarization measurements (Table 1).

3.2. AC electrochemical results

Nyquist and Bode plots of mild steel after 2 h of immersion in solutions containing different concentrations of AAOA inhibitor are given in Fig. 4.

As can be seen in Fig. 4, the Nyquist plots have the form of depressed semicircles with the center under the real axis indicating a charge transfer process. The depressed semicircle form is characteristic of a dispersion in frequency and has been attributed to different physical phenomena such as roughness and inhomogeneities of solid surfaces during corrosion [19].

For concentrations of inhibitor lower than 0.27×10^{-5} M, there are two capacitive arcs in the EIS Nyquist plots and two time constants in the EIS Bode plots (Fig. 4a and c). The continuous increase in the diameter of the Nyquist semicircle and in the impedance module with the inhibitor concentration is in agreement with the former DC measurements. In the Bode θ versus log f plots, it can be seen that these time constants emerge at a frequency about 20 and 4×10^3 Hz and can be attributed to the double layer capacitance and to the presence of a porous inhibitor film, respectively [17,20]. The value of the maximum phase angle of the first time constant is increased due to the increase of the inhibitor concentration. This is in accordance with the fact that the product only acts blocking part of the active surface of the electrode (Section 3.1).

At inhibitor concentrations higher than 0.27×10^{-5} M, the second time constant can be clearly seen (Fig. 4c and d). The low frequency time constant could be related to the corrosion process at those areas where the electrolyte penetrates through the inhibitor film pores [21]. At this range of inhibitor concentration, the value of the maximum phase angle of the low frequency time constant remains constant, indicating that it could be related to the formation of a protective film. The existence of a high frequency time constant is in accordance with the presence of a thin isolating and protective inhibitor film over the surface [9]. This is in accordance with the increase in the anodic slope observed on the polarization curves at concentrations higher than 0.27×10^{-5} M (Fig. 3).

The frequency at the maximum of the imaginary component of the impedance, f′, can be used as a measure of the intrinsic reactivity of the steel surface as it is the inverse of the time constant for the process represented by the low frequency semicircle in the Nyquist plot [22]. As shown in Table 3, a great drop in f′ occurs for concentrations of AAOA higher than 0.27×10^{-5} M. This decrease could correspond to chemisorption of the organic compound to the steel surface [17] in agreement with the results obtained from polarizations curves, where a change in the adsorption mechanism of the studied inhibitor is suggested.

Electrical equivalent circuits are generally used to model the electrochemical behavior of real systems. When modeling corrosion problems, ideal capacitors are frequently replaced by Constant Phase Elements (CPE) representing leaky or non-ideal capacitors with a view to compensating for non-homogeneity in the system [23]. The impedance of a CPE is described by the following expression:

$$Z_{CPE} = Y^{-1}(i\omega)^{-n} \quad (4)$$

where Y is proportional to the capacitance of the corroding system [24], i is $\sqrt{-1}$, ω is $2\pi f$, and n represents a phase shift. For example, a rough or porous surface can cause a double-layer capacitance to appear as a CPE with an n value between 0.9 and 1. For $n = 0$, Z_{CPE} represents a resistance with $R = Y^{-1}$, for $n = 1$ a capacitance with

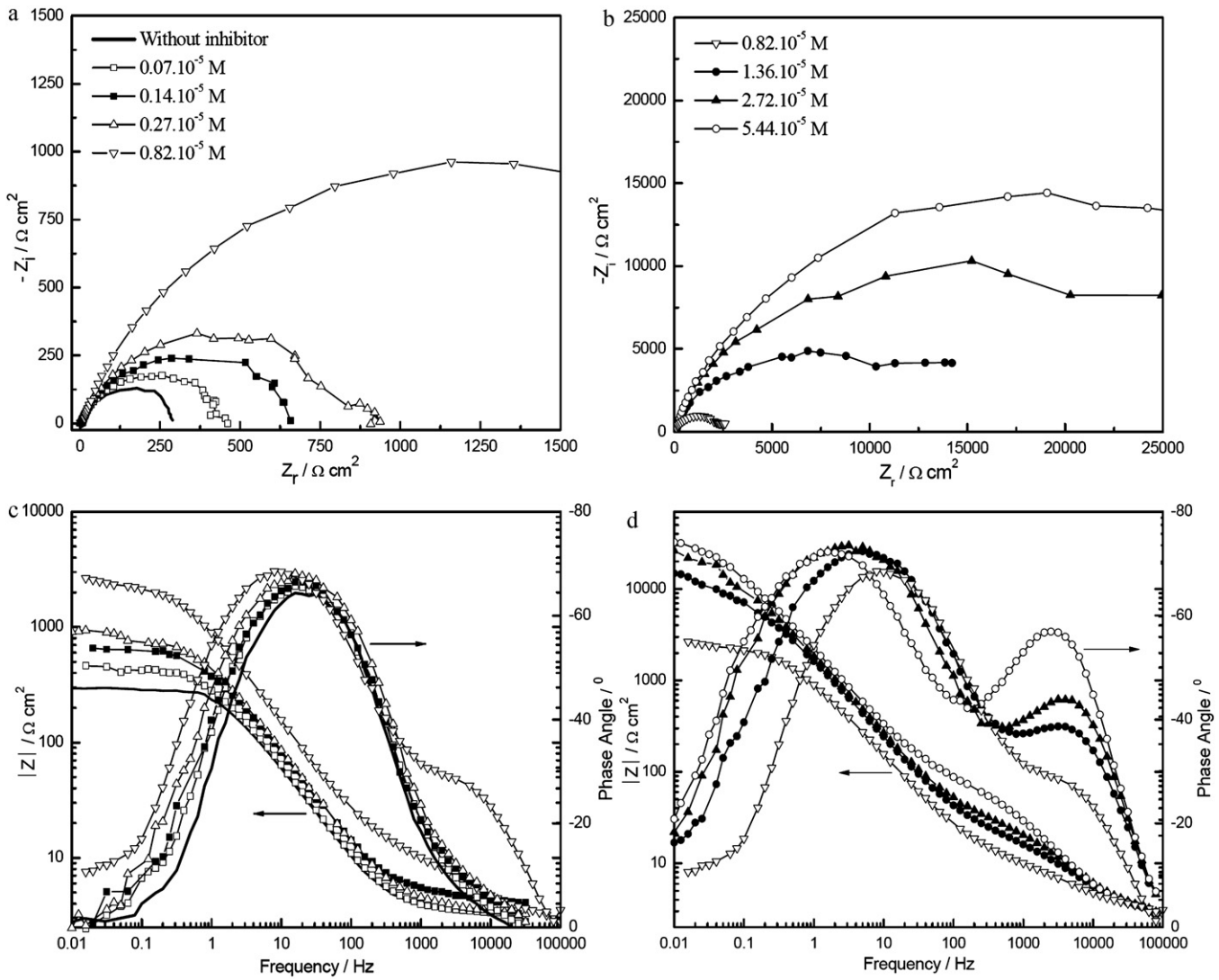

Fig. 4. Nyquist (a and b), and Bode (c and d), plots of mild steel exposed in a CO_2-saturated 5% NaCl solution with different concentrations of inhibitor: (—) 0 M, (□) 0.07×10^{-5} M, (■) 0.14×10^{-5} M, (△) 0.27×10^{-5} M, (▽) 0.82×10^{-5} M, (●) 1.36×10^{-5} M, (▲) 2.72×10^{-5} M and (○) 5.44×10^{-5} M.

$C = Y^{-1}$, for $n = 0.5$ a Warburg element and for $n = -1$ an inductance with $L = Y^{-1}$.

The corresponding electrical equivalent circuit model for the mild steel in uninhibited solution is given in Fig. 5a, where R_s is the electrolyte resistance, R_{ct} is the charge transfer resistance, Y_{CPEdl} is proportional to the double layer capacitance C_{dl}, and n_{CPEdl} is the constant phase element exponent. The experimental results for concentrations lower than 0.27×10^{-5} M of the inhibitor could be modeled by a equivalent circuit representing a porous inhibitor film (Fig. 5b) [11,17,25], where R_1 is the resistance of the inhibitor film pores, Y_{CPE1} is proportional to the capacitance of the film C_F, and n_{CPE1} is the constant phase element exponent [20].

For samples corroded 2 h with 0.82×10^{-5} M of the corrosion inhibitor, the analysis of the impedance spectra is done using a simple equivalent circuit given in Fig. 5c. In this electrical circuit Z_W is a finite length Warburg impedance element that represents the diffusion of reactive species [26]. This impedance element is calculated by the equation:

$$Z_W = R_W(T_W i\omega)^{-n} \tanh[(T_W i\omega)^{-n}] \quad (5)$$

where R_W is the diffusion resistance, T_W represents the relation l_e^2/D_e, being D_e the effective diffusion coefficient of the reactive species and l_e the effective diffusion thickness, and the exponent n is equal to 0.5.

The equivalent circuit that is used to model impedance data for additions of inhibitor concentrations higher than 0.82×10^{-5} M is given in Fig. 5d. This model represents the existence of a porous bilayer inhibitor film taking into account diffusion processes within pores in the film: the inner layer is formed on the metal surface and the outer layer on top of the latter, both with different electrical properties. In this equivalent circuit Z_{CPE2} and R_2, and Z_{CPE1} and R_1 are related to the non-ideal capacitance and to the pore resistances of the outer and inner layer of the inhibitor film, respectively.

As a representative example, the fitting results for the impedance spectra corresponding to 0.27, 0.82 and 2.72×10^{-5} M inhibitor concentrations are shown in Fig. 6. In all cases the fitted data have an average error lower than 5%. It can be seen that the proposed models are well representative of the phenomena which may occur in the investigated system, both in the high frequency and in the low frequency part of the spectrum. The values of impedance parameters obtained by fitting the impedance data are listed in Tables 4 and 5.

The inhibition efficiencies of the studied inhibitor are calculated from R_{ct} values at different concentrations using the following

Table 4
Circuit parameters of the modeling of impedance spectra for mild steel in CO_2 solution containing different concentrations of the inhibitor at 25 °C. Concentration ($\times 10^{-5}$ mol dm^{-3}), R (Ω cm^2), Y_{CPE} (Ω^{-1} cm^{-2} s^n 10^{-6}), EI (%).

Concentration	R_s	Y_{CPE2}	n_{CPE2}	R_2	Y_{CPE1}	n_{CPE1}	R_1	Y_{CPEdl}	n_{CPEdl}	R_{ct}	EI
0	3.3	–	–	–	–	–	–	464	0.85	309	–
0.07	3.5	–	–	–	386	0.83	3.4	184	0.82	462	34
0.14	3.4	–	–	–	352	0.79	4.4	168	0.89	614	49
0.27	3.6	–	–	–	308	0.79	6.1	139	0.87	1006	66
0.82	3.3	–	–	–	41	0.82	12.6	165	0.85	3234	90
1.36	3.3	11.7	0.91	10.6	36	1	81.9	176	0.88	12945	98
2.72	3.4	11.1	0.90	18.4	35	1	109	172	0.86	17004	99
4.08	3.5	10.8	0.91	25.7	36	1	139	141	0.83	25131	99
5.44	3.5	7.3	0.93	34.8	35	1	270	147	0.88	32543	99

equation [20]:

$$IE(\%) = \frac{R_{ct} - R_{ct}^0}{R_{ct}} \times 100 \quad (6)$$

where R_{ct} and R_{ct}^0 are the charge transfer resistance for solutions with and without inhibitor, respectively. The results obtained are

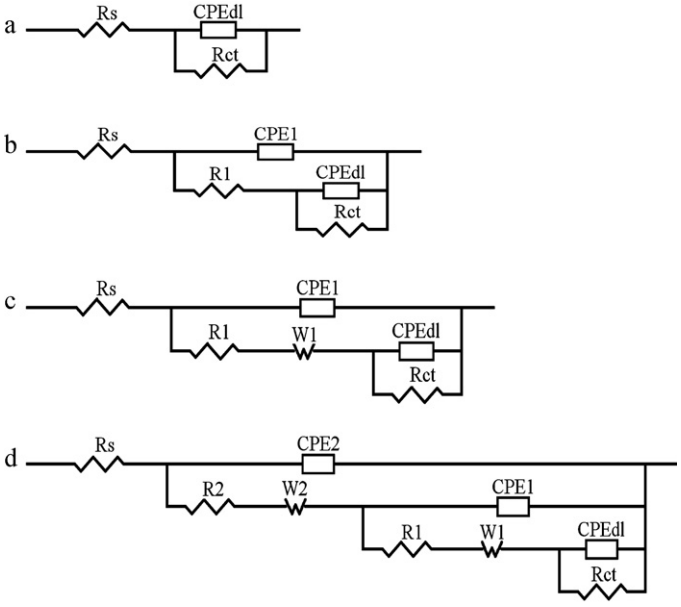

Fig. 5. (a–d) Different equivalent circuits used for the modeling of the impedance data.

Table 5
Circuit diffusion parameters from the modeling of impedance spectra for mild steel in a CO_2 solution containing different concentrations of the inhibitor at 25 °C.

Concentration ($\times 10^{-5}$ mol dm^{-3})	T_{W2} (s)	R_{W1} (Ω cm^2)	T_{W2} (s)	R_{W1} (Ω cm^2)
0.82	–	–	15.7	893
1.36	0.56	546	17.4	3270
2.72	0.75	783	24.2	6818
4.08	1.39	1360	30.6	10877
5.44	1.68	1758	34.6	14229

shown in Table 4. As can be seen in this table, the inhibition efficiencies, calculated from AC impedance results, show similar trend as the linear polarization resistance method and polarization curves. The values of R_1 increase with increasing concentration of inhibitor. These results suggest that the adsorbed inhibitor species increase the resistance of the dissolution reaction of metal or they simply block the reaction sites. On the other hand, Y_{CPE1} decrease with an increase in the inhibitor concentration.

The adsorption of an organic inhibitor on the metal–solution interface causes the gradual replacement of water molecules originally adsorbed on the electrode surface, $H_2O_{(ads)}$, by the organic molecules in the aqueous solution, $Org_{(sol)}$. This process is represented as [27]:

$$Org_{(sol)} + nH_2O_{(ads)} \leftrightarrow Org_{(ads)} + nH_2O_{(sol)}$$

where $Org_{(sol)}$ and $Org_{(ads)}$ are the organic molecules in the aqueous solution and the adsorbed molecules on the metallic surface, respectively, and n is the size ratio representing the number of water molecules replaced by one molecule of organic adsorbate. It can be assumed that the measured current is proportional to the number of available corroding sites remaining after blockage due

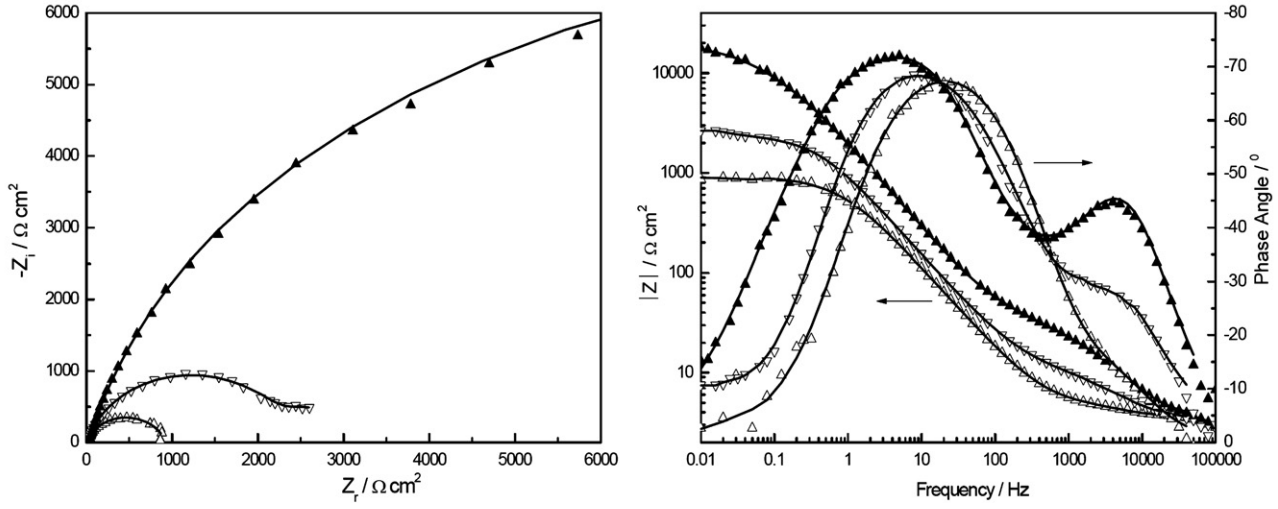

Fig. 6. EIS plots for mild steel at 25 °C: experimental data for (△) 0.27 × 10^{-5} M, (▽) 0.82 × 10^{-5} M and (▲) 2.72 × 10^{-5} M of inhibitor; (-) fitting results.

to inhibitor adsorption. Thus, the increase of R_1 and the decrease in Y_{CPE1} is attributed to the adsorption of the inhibitor compound on the metal surface, blocking active sites of the surface at low concentrations and leading to the formation of a protective film for concentrations higher than 0.82×10^{-5} M, decreasing the corrosion rate.

The thickness of the protective layer, d_{org}, is usually greater than that of water molecule. It can be related to C_1 by the following equation [28]:

$$d_{org} = \frac{\varepsilon_0 \varepsilon_r}{C_1} \propto \frac{\varepsilon_0 \varepsilon_r}{Y_{CPE1}} \quad (7)$$

where ε_0 is the permittivity of free space and ε_r is the relative dielectric constant. From this equation, it can be seen that a decrease in C_1 can be the result of a decrease in the local dielectric constant, which suggests that AAOA molecules are adsorbed at the metal/solution interface. Thus, a low capacitance may be the result of the replacement of water molecules at the electrode interface by organic inhibitor molecules of a lower dielectric constant. The larger inhibitor molecules reduce the capacitance through the increase of the film thickness [29].

As mentioned above, when the inhibitor is added at concentrations higher than 0.82×10^{-5} M, the protective film seems to be made up of two layers with different electrical properties. The resistance of the inner layer (R_1) is one order of magnitude higher than that of the outer one (R_2) (Table 4) which would suggest that the number of pores per unit of area and/or the pores size that could be penetrated by the electrolyte is smaller. This could be related to an inner layer with a higher molecular density as has been proposed previously by other authors [30]. This phenomenon could be associated to higher values of T_{W1} than T_{W2} (Table 5), which suggests that it is more difficult for ions to diffuse through pores within the inner layer. It might indicate that the inhibitor film is less porous or has pores with smaller effective diffusion thickness for high inhibitor concentrations. This results shows that AAOA corrosion inhibitor has a good performance of corrosion protection by forming more compact and less porous inhibitor films on the metal surface. Besides, Fig. 4 shows that the phase angle increases gradually with the inhibitor concentration. This could be related to the formation of a more compact film which has smaller pore size that hinders the passage of the reactive species. This is in accordance with the higher values of R_1 and R_2 observed.

Results are consistent with the fact that at inhibitor concentrations lower than 0.82×10^{-5} M, molecules adsorbs on the steel surface through an interaction between their polar head group and the iron atoms. In this range of concentration, molecules can be oriented perpendicularly to the surface forming admicelles and can also lay flat. In this last orientation, hydrocarbon chains can also interact with iron through the π electrons of the double bonds. The polar functions or reaction centers of the inhibitor can block the active sites which are accessible for corrosion, and the hydrocarbon chain can form a porous and very thin barrier between steel and medium, which impedes the access of corrosive ions to the metal surface. When the inhibitor concentration increases, it is possible that molecules change their orientation. Experimental results suggest that this could happen at 0.82×10^{-5} M of AAOA, when a porous monolayer could be formed and the self-assemble is better because of the presence of double bonds in the hydrocarbon chain that facilitates the interaction between molecules. This is in accordance with the increase of efficiency at high concentrations. At higher concentrations of the inhibitor, the efficiency reaches a steady state which could indicate that the surface is saturated and a protective bilayer is formed. This is in accordance with others authors suggest [31].

From a practical point of view, in CO_2 containing brines the recommended concentration of an inhibitor should be one that assures a minimum efficiency of 95%. It can be seen that in the selected experimental conditions this minimum concentration would be 1.36×10^{-5} M.

3.3. PM-IRRAS studies of adsorbates

PM-IRRAS spectra were recorded after electrodes were immersed 2 h at open circuit potential in an aqueous inhibited solution containing 0.82×10^{-5} M of AAOA and 5% NaCl saturated with CO_2 at 25 °C. It should be noted that at this concentration of inhibitor previous results indicated that a monolayer is adsorbed on the metal surface. Fig. 7 shows PM-IRRAS spectra of AAOA adsorbed on a mild steel substrate. For comparison purposes, the IR spectrum of a KBr disc of AAOA after the synthesis is added. In this spectrum, the NH peak between 3500 and 3100 cm^{-1} and the carbonyl peak at 1636 cm^{-1} can be seen. It is important to note the absence of the peak of the C=N bond, which indicates that the cyclization of the amido-amine does not occur [32]. The peaks at 2924 and 2853 cm^{-1} correspond to the characteristic symmetric and asymmetric C–H stretching vibrations of the CH_2 groups in the inhibitor chain, respectively. The CH_3 stretching symmetric and asymmetric absorption bands are at 2955 and 2872 cm^{-1}, respectively. As is expected, the IR spectrum of the neat inhibitor and the PM-IRRAS spectrum obtained from the surface of the coupon exposed to inhibitor have similar peaks. There are no changes in the position of stretching bands of the hydrocarbon chain, remaining at 2959 and 2882 cm^{-1} for the CH_3 asymmetric and symmetric stretching bands, and at 2927 and 2855 cm^{-1} for the CH_2 asymmetric and symmetric stretching bands, respectively.

A close examination of the PM-IRRAS spectra for mild steel samples exposed to the AAOA displays some differences respect to the spectrum of the neat compound. It can be seen that there is a reduction of the relative intensity of NH peak between 3400 and 3200 cm^{-1}, and the peak width decreases. The peak at 1462 cm^{-1} is probably due to the CH_3 asymmetric bending, possibly with a contribution from the CH_2 scissor on the high wavenumber side of the 1462 cm^{-1} peak [33]. The peak at 1642 cm^{-1} can be associated to the amide band. Several new peaks appear and others change or increase their relative intensity in the range of 1250–1020 cm^{-1}. These peaks could be assigned to C–N and/or C–O stretching vibrations of the corrosion inhibitor. Because of that, the adsorption of AAOA on mild steel could occur through the primary or secondary amine and/or the amide functional groups.

Since PM-IRRAS measurements were taken under *ex situ* conditions, it was possible to wash the sample after obtaining the first spectrum and then acquire a second one. Fig. 7 shows the spectrum obtained after the washing procedure. It can be seen that despite the sample is rinsed with ethanol, the corrosion inhibitor still remains on the steel surface. The spectrum is very similar to that obtained before the washing step. The same peaks with slightly lower relative intensity are observed. This result supports the assumption that the AAOA molecules are chemisorbed [33], which is in accordance with results obtained by the electrochemical techniques.

By PM-IRRAS spectroscopy is possible to evaluate molecular orientation of adsorbed molecules on metal surfaces. Molecular orientation could be important to understand the high efficiency of this inhibitor. The wave number position of the CH_2 asymmetric peak in Fig. 7 (2927 cm^{-1}) indicates that the AAOA monolayer has an amorphous, heavily disordered, liquid like structure (a perfectly ordered monolayer would give 2918 cm^{-1}) [25,34]. The liquid state of the hydrocarbon chains and their distribution close to random may be a consequence of the surface roughness [35]. This is in accordance with the values of n obtained from EIS method (Table 4) which show roughness and inhomogeneities on steel surface. Although the inhibition efficiency of AAOA in this experiment

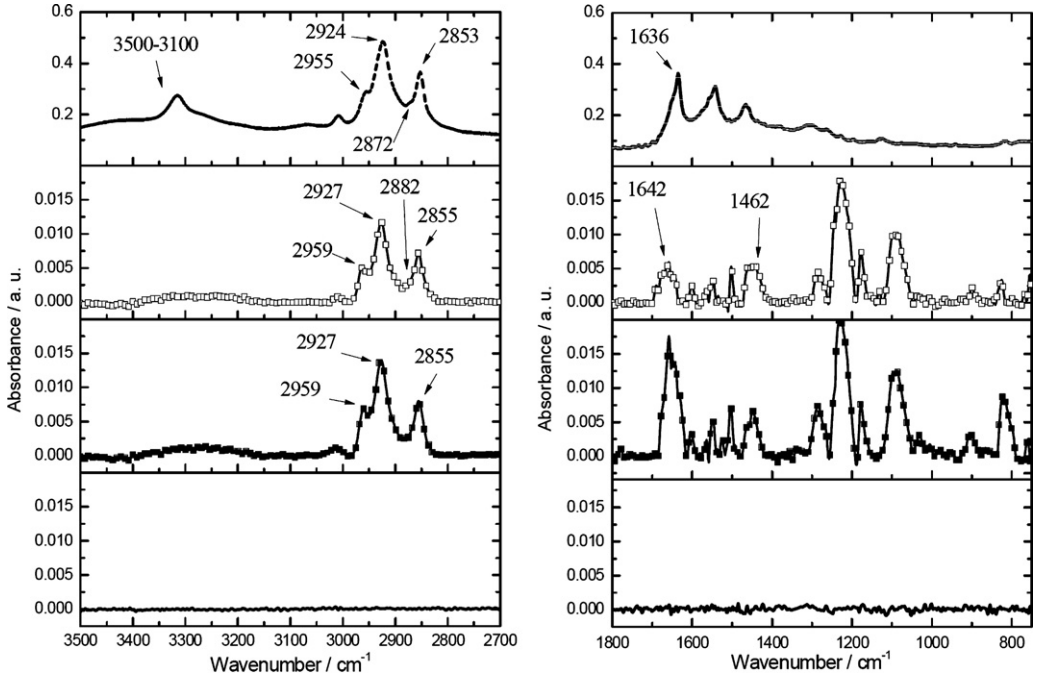

Fig. 7. PM-IRRAS spectra of the corrosion inhibitor on carbon steel sample collected after the electrode was immersed 2 h at E_{corr} in an aqueous inhibited solution containing 0.82×10^{-5} M of the inhibitor and 5% NaCl saturated with CO_2 at 25 °C: ((—) before immersion (blank), (■) spectrum obtained after the immersion time, (□) spectrum obtained after the washing), and IR spectrum of a KBr disc of AAOA after the synthesis (- - -).

at 0.82×10^{-5} M is high (90% approximately), some minor dissolution of the carbon steel occurs. Under these conditions, it is not possible to obtain a well-ordered monolayer. It could be expected that some inhibitor molecules form hemicelles or admicelles, and others are arranged horizontally to the steel surface. This leads to the formation of a thinner and more porous hydrophobic barrier than that one perfectly ordered. As a consequence, lower inhibition efficiency is expected.

By PM-IRRAS, it can be demonstrated that the adsorption of the AAOA molecules could occur due to the formation of links between the d orbital of iron atoms, involving the displacement of water molecules from the metal surface, and the lone sp^2 electron pairs present on the N and/or O atoms. This could be possible because of the chemisorption process that occurs between AAOA molecules and mild steel surface.

4. Conclusions

The adsorbed inhibitor molecules are assumed to retard corrosion by reducing the number of available surface sites for corrosion and also by decreasing the rate of the corrosion reactions. The organic molecules of AAOA act by blocking surface sites at low concentrations and by modifying the adsorption mechanism forming a protective barrier against corrosive ions at high concentrations. This protective film becomes less porous with the increase of concentration of the inhibitor. Also, PM-IRRAS spectrum of the steel surface reveals the presence of a protective surface layer over the metal exposed to a CO_2 saturated solution.

The AAOA corrosion inhibitor exhibits high corrosion efficiencies as a mixed-type inhibitor with the predominant influence on the anode process for the mild steel corrosion in CO_2 saturated solution at 25 °C. Excellent agreement between the inhibition efficiencies calculated using the three electrochemical studies is obtained.

PM-IRRAS results demonstrate that the inhibitor is chemisorbed to surface steel via formation of links between the d orbital of iron atoms and N or O atoms. Moreover, these measurements show that the AAOA monolayer has a heavily disordered structure.

Acknowledgements

This work was supported by the Argentine Research Council for Science and Technology (CONICET) and the University of Mar del Plata. The authors are grateful to Melanie Wilhelm and Michael Maxisch for their assistance during the PM-IRRAS measurements. M. Desimone acknowledges the Deutsche Akademische Austauschdienst (DAAD) for award of exchange scholarship.

References

[1] J.A. Martin, F.W. Valone, Corrosion 41 (1985) 281.
[2] R.N. Butler, J.D. Thornton, P. Moynihan, J. Chem. Res. (S) (1981) 84.
[3] V. Jovancicevic, S. Ramachandran, P. Prince, Corrosion 55 (1999) 449.
[4] D.A. López, S.N. Simison, S.R. de Sanchez, Electrochim. Acta 48 (2003) 845.
[5] T. Hong, Y.H. Sun, W.P. Jepson, Corrosion Sci. 44 (2002) 101.
[6] C.H. Tsai, F. Mansfeld, Corrosion 49 (1993) 726.
[7] K. Wapner, M. Stratmann, G. Grundmeier, Int. J. Adhes. Adhes. 28 (2007) 59.
[8] F.G. Liu, M. Du, J. Zhang, M. Qiu, Corrosion Sci. 51 (2009) 102.
[9] O. Olivares-Xometl, N.V. Likhanova, M.A. Dominguez-Aguilar, J.M. Hallen, L.S. Zamudio, E. Arce, Appl. Surf. Sci. 252 (2006) 2139.
[10] H.H. Hassan, E. Abdelghani, M.A. Amin, Electrochim. Acta 52 (2007) 6359.
[11] M. Knag, K. Bilkova, E. Gulbrandsen, P. Carlsen, J. Sjoblom, Corrosion Sci. 48 (2006) 2592.
[12] D.A. Jones, Principles, Prevention of Corrosion, Macmillan Publishing Company, 1991.
[13] C. Cao, Corrosion Sci. 38 (1996) 2073.
[14] S.A. Ali, A.M. El-Shareef, R.F. Al-Ghamdi, M.T. Saeed, Corrosion Sci. 47 (2005) 2659.
[15] X. Liu, P.C. Okafor, Y.G. Zheng, Corrosion Sci. 51 (2009) 744.
[16] X.Y. Zhang, F.P. Wang, Y.F. He, Y.L. Du, Corrosion Sci. 43 (2001) 1417.
[17] I. Esih, T. Soric, Z. Pavlinic, Br. Corrosion J. 33 (1998) 309.
[18] J. Wang, C. Cao, J. Chin, Soc. Corros. Protect. 16 (1996) 9.
[19] K. Jüttner, Electrochim. Acta 35 (1990) 1501.
[20] G. Zhang, C. Chen, M. Lu, C. Chai, Y. Wu, Mater. Chem. Phys. 105 (2007) 331.
[21] L.D. Paolinelli, T. Pérez, S.N. Simison, Corrosion Sci. 50 (2008) 2456.
[22] F.B. Growcock, Chem. Technol. (1989) 564.
[23] ZPlot for Windows, Electrochemical Impedance Software Operating Manual, Scibner Associates Inc., Southern Pines, NC, 1998.
[24] C.H. Hsu, F. Mansfeld, Corrosion 57 (2001) 747.

[25] S. Ghareba, S. Omanovic, Corrosion Sci. 52 (2010) 2104.
[26] S.R. Taylor, E. Gileadi, Corrosion 51 (1995) 664.
[27] J.O.M. Bochris, D.A.J. Swinkels, J. Electrochem. Soc. 111 (1964) 36.
[28] F. Bentiss, M. Lebrini, M. Lagrenee, Corrosion Sci. 47 (2005) 2915.
[29] P. Li, J.Y. Lin, K.L. Tan, J.Y. Lee, Electrochim. Acta 42 (1997) 605.
[30] Y.J. Tan, S. Bailey, B. Kinsella, Corrosion Sci. 38 (1996) 1681.
[31] M.M. Osman, R.A. El-Ghazawy, A.M. Al-Sabagh, Mater. Chem. Phys. 80 (2003) 55.
[32] X.Y. Liu, S.H. Chen, H.Y. Ma, G.Z. Liu, L.X. Shen, Appl. Surf. Sci. 253 (2006) 814.
[33] W.H. Durnie, B.J. Kinsella, R. De Marco, A. Jefferson, J. Appl. Electrochem. 31 (2001) 1221.
[34] S.-Y. Lin, C.-h. Chen, Y.-C. Chan, C.-M. Lin, H.-W. Chen, J. Phys. Chem. B 105 (2001) 4951.
[35] I. Zawisza, G. Wittstock, R. Boukherroub, S. Szunerits, Langmuir 23 (2007) 9303.